

Winebrenner, D. P., Arthern, R. J., and Shuman, C. A. (2001), Mapping Greenland accumulation rates using observations of thermal emission at 4.5-cm wavelength, *J. Geophys. Res.*, 106( D24), 33919– 33934, doi:10.1029/2001JD900235.

<https://doi.org/10.1029/2001JD900235>

Copyright 2001 by the American Geophysical Union

Access to this work was provided by the University of Maryland, Baltimore County (UMBC) ScholarWorks@UMBC digital repository on the Maryland Shared Open Access (MD-SOAR) platform.

**Please provide feedback**

Please support the ScholarWorks@UMBC repository by emailing [scholarworks-group@umbc.edu](mailto:scholarworks-group@umbc.edu) and telling us what having access to this work means to you and why it's important to you. Thank you.

# Mapping Greenland accumulation rates using observations of thermal emission at 4.5-cm wavelength

Dale P. Winebrenner and Robert J. Arthern<sup>1</sup>

Applied Physics Laboratory, University of Washington, Seattle, Washington, USA

Christopher A. Shuman

Earth System Science Interdisciplinary Center, University of Maryland, College Park, Maryland USA

**Abstract.** Accurate predictions of sea level rise over the coming century will require improved knowledge of the processes controlling accumulation on the great ice sheets. The sparsity of accumulation rate observations, both temporally and spatially, hinder development of this understanding. We introduce a new method to observe accumulation rates (averaged over roughly a decade) using satellite observations of microwave emission at 4.5-cm wavelength, focusing in this paper on Greenland. At this wavelength, scattering by the grain fabric in firn is unimportant relative to quasi-reflection from density (and thus dielectric permittivity) stratification. We show observationally a strong link between random firn density stratification, on scales of millimeters to centimeters, and accumulation rate. We then show theoretically how the observed density stratification can produce and is consistent with observations of polarization of 4.5-cm-wavelength emission. We employ observations from the Scanning Multichannel Microwave Radiometer (SMMR) and previously published ground observations of accumulation rates in Greenland to complete specification of the relationship between accumulation rate and polarization. The relationship is sufficiently accurate to serve as a basis for mapping accumulation rate fields. We compare our satellite-derived maps with previously published maps based on syntheses of ground data. We find broad agreement between the two types of maps, though the satellite-derived map indicates more strongly the importance of topography and prevailing weather patterns in determining detailed accumulation rate patterns. Finally, we discuss possible refinements and the prospects for improved satellite-derived maps based on a new generation of sensors about to be launched.

## 1. Introduction

The spatial patterns of mass accumulation rate over the great ice sheets, and temporal changes in those patterns, are essential information for understanding mass balance dynamics. The accumulation rate field and gross geometry of an ice sheet determine first-order estimates of ice sheet flow, the so-called balance velocities [Joughin *et al.*, 1997; Bamber *et al.*, 2000]. Uncertainties in accumulation rate fields and their decadal variability are among the principal error sources in mass

balance estimates, and thus estimated contributions to sea level change, for Greenland [Thomas *et al.*, 2000] and Antarctica [Wahr *et al.*, 2000]. Perhaps most significantly, understanding how ice sheets will respond to climate variations, whether natural or anthropogenic, requires an understanding of the interaction of topography and meteorological patterns [Chen and Bromwich, 1999; Krinner *et al.*, 1997; Oerlemans and Hoogenboom, 1989]. However, tests of theory for this interaction are presently severely limited by sparsity of available data (due to logistical constraints). Satellite observations of accumulation rate fields, at resolutions of a few tens of kilometers and averaging over known temporal periods, would thus be highly valuable, even if limited to dry snow zones.

Motivated along these lines, Zwally [1977] combined radiative transfer theory for scattering from ice grains in the upper few meters of firn with a model for isothermal

<sup>1</sup>Now at British Antarctic Survey, Cambridge, England United Kingdom.

ice grain growth in the dry snow zone [Gow, 1971], to link firn microwave emission to accumulation rate and temperature. The length scale of absorption for microwaves in water ice ( $I_h$ ) at terrestrial temperatures is on the order of tens of meters, while the dielectric constant (relative to vacuum or air) is closely approximated by 3.2 [Mätzler, 1987]. On length scales  $\lesssim 10^{-3}$  m, near-surface firn in dry snow zones can be viewed as a granular medium of ice grains (or particles) embedded in air, with a volume fraction of ice ranging from 0.25 to 0.45 in the first meter of depth to roughly 0.8 at depths of a few tens of meters [Benson, 1971; Alley, 1988]. Thus at microwave wavelengths of  $\lesssim 1\text{--}2$  cm (10 times typical grain sizes), it is reasonable (and arguably successful, see below) to model near-surface perennially dry firn as a low-loss granular scattering material in a layer of significant optical depth. The approximately linear (though highly temperature dependent) increase in mean cross sectional ice grain area with time (and thus, via accumulation rate, depth) [Gow, 1971; Kieffer, 1990] theoretically links properties of the scattering layer, including its emissivity, to geophysical properties.

Zwally's early work led directly to the method of Zwally and Giovinetto [1995] (see also Vaughan et al. [1999]) for mapping ice sheet accumulation rates using a combination of emission observations at 1.6-cm wavelength (i.e., frequency 19 GHz) and ground-based accumulation rate observations. The same work led also to at least two methods for inferring dry snow zone accumulation rates from microwave backscattering observations at 2- and 6-cm wavelengths [Forster et al., 1999; Drinkwater et al., this issue]. In all these methods the putative physics linking microwave signatures with accumulation rate depends on a reliable relationship between ice grain sizes at the relevant firn depths and accumulation rate. However, at 1- to 2-cm-wavelength microwave interaction with the firn is likely limited to the upper 2–5 m beneath the snow surface [Zwally, 1977]. Temperature in this depth range is not isothermal, but rather is strongly seasonal [Paterson, 1994]; thus the relationship between grain size, (mean surface) temperature, and accumulation rate given by Gow [1971] for firn at greater (nearly isothermal) depths may require modification for the ice grains thought to determine the relevant microwave signatures [Alley, 1987; Kieffer, 1990; Abdalati and Steffen, 1998]. Perhaps partly for this reason, all of the methods above must use information from ground-based measurements to calibrate inversion model parameters empirically.

An alternative possibility exists, however, for sensing dry snow zone accumulation rates based on different physics and emission at longer wavelengths. For increasing wavelength,  $\lambda$ , greater than roughly 10 times the ice particle size (i.e., about 2 cm in this case), scattering from particles (now in the Rayleigh regime) decreases as  $\lambda^{-4}$ . Wave propagation in the granular medium becomes increasingly like propagation in a "ho-

mogenized" medium with effective dielectric properties that depend on the volume fraction of ice particles, i.e., on the density of the firn [Mätzler, 1987]. Although weak particle scattering may yet dominate backscattering (at angles off nadir), its effects on total power reflectivity of the firn (and thus, via Kirchhoff's law, emissivity) must compete with those from stronger, nearly wavelength-independent processes, e.g., reflection and scattering from the air/snow interface. Whatever influence particle scattering has on emissivity at 1.6-cm wavelength, we expect this influence to be diminished at 3- to 6-cm wavelength by a factor of roughly 16 or more. However, firn also displays structure in its density [Benson, 1971; Alley, 1988] and therefore its effective dielectric properties [Mätzler, 1987], in the form of layering on scales of  $\approx 10^{-3} - 10^0$  m, at depths from the surface to several meters. Because density often changes abruptly across layer interfaces [Benson, 1971; Alley, 1988], many layer interfaces constitute abrupt, reflecting dielectric interfaces. Although the dielectric contrasts between layers are weak, the low absorption in firn allows reflections from many such layers to affect emissivity cumulatively and predominantly at 4.5-cm wavelength [Surdik and Fily, 1995].

West et al. [1996] tested one version of this mechanism using data from four East Antarctic dry snow sites with differing accumulation rates and radiometric properties, at which 5-cm-resolution density profiles and 6-cm-wavelength emission observations were available. They computed emission by idealizing the firn as a random stack of planar, centimeter-scale dielectric layers with properties determined by the density profiles and temperature; the scale of the model layers was set by the resolution of the ground data, published accounts of firn layering, and visual observations in situ. The computed average emission (of an ensemble of statistically similar stacks) agreed well with observed vertically and horizontally polarized emission versus incidence angle at each site. The variation with accumulation rate of the polarization of emission, in particular, agreed with that noticed earlier by Rott [1989] and Rott et al. [1993]. Arthern et al. [1997] and Winebrenner and Arthern [1998] therefore examined a larger collection of published 5-cm-resolution depth profiles at Greenland and Antarctic sites where accumulation rate estimates were available and, empirically, found linear relationships between accumulation rates and mean centimeter-scale layer thicknesses inferred from 5-cm-resolution data (with slightly differing slopes for the two ice sheets). Use of the empirical relationship for Antarctica, together with computations of emission polarization at 4.5-cm wavelength (including independent information about thin snow crusts) and observations from the Scanning Multichannel Microwave Radiometer (SMMR) produced a map of Antarctic accumulation rates, which compares favorably with, for example, a variety of ground-based observations around Taylor Dome, East Antarctica [Morse et al., 1999].

However, a merely empirical relationship between accumulation rate and a quantity interpreted as centimeter-scale layer thickness is, in our view, unsatisfactory; because the physical cause of the putative relationship is obscure, neither the conditions under which the relationship is reliable nor its sensitivity to (or correction for) variations in parameters other than the accumulation rate can be assessed directly. We therefore undertook field work in the vicinity of the Greenland Summit during May 1998 to observe layering dependence on accumulation rate and snow crusts and to clarify the physics underlying that dependence. Our field observations and analysis illuminate relationships between accumulation rate and layering on scales ranging from millimeters to decimeters, as well the role of layering in determining 3- to 6-cm microwave emission.

Thus in section 2 we analyze density profiles with 2-cm resolution from locations in Greenland and West Antarctica which span a range of accumulation rates; we show that in addition to the well-known summer/winter density variations (on decimeter scales, in these cases), the variance of density stratification on scales  $\gtrsim 1$  mm to 4 cm correlates strongly with accumulation rate. In section 3, we show that it is this fine-scale density stratification that must be responsible for the observed relationship between the accumulation rate and the polarization of emission at 4.5-cm wavelength and that the form of the resulting theoretical relationship is consistent with observations. In section 4, we use a provisional, observationally specified relationship for Greenland to produce a map of accumulation rate in the dry snow zone and discuss its features relative to accumulation variations known from ground observations. However, the physics relating fine-scale stratification and accumulation rate remains to be quantitatively explained. We discuss the way forward to a completely physically based method for accumulation rate estimation from satellite data, as well as the prospects afforded by new observations from the Advanced Microwave Scanning Radiometer, in the final section.

## 2. Firn Density Stratification and Accumulation Rate

### 2.1. Description of the Data

The density versus depth data analyzed here were collected using the method described in detail by *Shuman et al.* [1995; 1998; this issue] in connection with stable isotope profiling and seasonal temperature history reconstruction. (Density profiles constitute essential supporting data for isotope and temperature work but are the primary data for this study.) Briefly, the method consists of (1) digging a 2- to 4-m-deep snow pit, wherever possible with a companion pit separated from the first by a (roughly) 30-cm-thick snow wall, oriented so that the solar illumination enables detailed stratigraphic mapping of that wall, to aid interpretation of

quantitative data; (2) use of a stainless steel penetrator and cutter box to extract known snow volumes of 2-cm thickness, centered in depth at 2-cm intervals, beginning 1 cm beneath the air/snow surface, thus yielding profiles 100–200 samples in length; (3) bagging and labeling of samples as collected in a sequence of clean, inert, preweighed, watertight-sealing plastic bags; and (4) prompt weighing of each bag and snow sample in a field laboratory and subsequent computation of density. Density variations within the first few centimeters of the snow surface can vary wildly and are difficult to sample; we have therefore edited the density series used here to begin at a depth of 4 cm. The estimated density measurement error for the remaining individual samples, for typical dry polar firn densities, is 5%. The accumulation rate is estimated for the point location of the pit, averaged over only the time spanned by the depth of the pit, by using stable isotope series to establish a depth-age scale and densities to convert depth to mass.

The particular data for this study come from 12 sites with similar mean annual temperatures but with accumulation rates that vary by nearly a factor of 5. Table 1 gives locations and accumulation rates for seven sites in the vicinity of the Greenland Summit at which data were acquired during May 1998 and 1995 and for five sites in the vicinity of Siple Dome, West Antarctica, at which data were acquired during the austral spring of 1996. Decadal-mean surface temperature in a region encompassing all of the Greenland sites has been reported to be  $-30^{\circ} \pm 2^{\circ}\text{C}$  [*Clausen et al.*, 1988]; temperature records in the vicinity of Siple Dome are shorter but indicate mean surface temperatures of  $-22^{\circ} \pm 0.5^{\circ}\text{C}$  [*Shuman and Stearns*, 2001]. To minimize the errors inherent in point estimates of accumulation, we have used only pit records containing at least 3 years of accumulation, with one exception: The record for site G in West Antarctica contains only 2 years of accumulation, but it is the only Antarctic site for which the accumulation rate falls within the range spanned by the Greenland sites; it thus provides a first indication of whether geographically varying factors other than accumulation rate affect density stratigraphy. Estimated accumulation rates range from  $285 \text{ kg m}^{-3} \text{ yr}^{-1}$  approximately 60 km southwest of the Greenland Summit to  $62 \text{ kg m}^{-3} \text{ yr}^{-1}$  in a particularly low-accumulation region near Siple Dome. Note that accumulation at GISP-2 preceding the 1995 observations was significantly lower than that immediately preceding the 1998 observations at the same site; we show below that fine-scale stratigraphy may reflect this temporal variability as well.

Finally, the wavelet analysis we employ here is facilitated by first removing the mean and linear trend from the profiles of density versus depth, i.e., by detrending. Detrending has no effect on estimates of wavelet power spectra (compare below), but it reduces abrupt changes in the periodic extensions of the density series on which wavelet analysis operates; it therefore reduces

Table 1. Data Site Characteristics

Site	Year	Location	Accumulation rate, kg m <sup>-2</sup> a <sup>-1</sup>	2-cm-scale variation, (kg m <sup>-3</sup> ) <sup>2</sup> a
GISP-2 Pit 1	1998	72.5758 N, 38.5276 W	265.2	293.2
GISP-2 Pit 2	1998	72.5843 N, 38.4227 W	263.8	210.8
GISP-2/95	1995	72.5758 N, 38.5276 W	190.7	327.7
Kenton	1998	72.3717 N, 38.6598 W	271.0	252.0
GRIP	1998	72.5779 N, 37.6465 W	259.1	385.6
North	1998	73.4998 N, 38.5000 W	188.4	423.0
Southwest	1998	72.1999 N, 40.5003 W	285.2	176.6
B	1996	81.6597 S, 148.8139 W	127.1	607.8
E	1996	81.3530 S, 148.2994 W	153.4	595.8
F	1996	81.9074 S, 149.3415 W	62.4	1270.2
G	1996	81.5711 S, 148.6329 W	224.0	249.4
I	1996	81.6375 S, 148.7634 W	143.2	597.9

<sup>a</sup>Unbiased estimates of  $P_W(2\text{ cm})$  (see section 2.2).

possible artifacts in the multiresolution analysis that we use to look for abrupt changes at seasonal transitions. We show this processing explicitly for one of our profiles below and in all cases perform our actual analysis only on detrended profiles.

## 2.2. Wavelet Methods

The density of firn at a given depth depends on the season in which the original snow was deposited and on intraseasonal scouring, deposition, and weathering events [Benson, 1971; Alley, 1988; Steffen *et al.*, 1999] (see also the data below). Firn density profiles therefore vary on a wide range of depth scales, from the decimeter scales characteristic of annual and seasonal effects to centimeter and millimeter scales characteristic of hoar events and firn crusts. Any density (and thus dielectric) variation within a depth interval that is short compared to a radiation wavelength, be it a seasonal transition or a crust, can produce a reflection and is thus significant to understanding emission at that wavelength. Slower variations with depth, however, are ineffective [Brekhovskikh and Godin, 1998]. Thus it is crucial to quantify the “shape” of annual and seasonal density variations, and in particular whether seasonal density changes are “sharp” on scales of a few centimeters or less, as well as random fine-scale variations due to weathering.

Classical spectral analysis is poorly suited to analysis of data series containing localized “events,” whereas analysis of such series using wavelets has proven effective [Percival and Walden, 2000]. Briefly, wavelet analysis decomposes data series into components that correspond to changes of data averages on varying scales. Such analysis quantifies not only the data variance on various scales but also the locations in the original series at which changes on those scales occur. This is precisely what we need for assessment of the influences of annual, seasonal, and random intraseasonal density variations on emission.

Certain characteristics of our data set drive the selection of specific wavelet analysis methods. The data

series are short (only 96–98 points in all but one case), their length is not equal to a power of 2, and they are not periodic. These facts complicate analysis using the simple discrete wavelet transform. Use of the Maximal Overlap Discrete Wavelet Transform (MODWT), however, allows optimal use of data in such series [Percival and Walden, 2000]. Choice of a zero-phase filter for the fundamental wavelet filter in the analysis permits alignment of wavelet transform coefficients with the original data series to see clearly where events on given scales occur; for this reason and other reasons we choose the Daubechies Least-Asymmetric, eighth-order (LA(8)) wavelet.

Let us represent a real-valued data series consisting of  $N$  regularly spaced samples, with sampling interval  $\delta$ , by the components  $X_0, X_1, \dots, X_{N-1}$  of an  $N$ -dimensional vector  $\mathbf{X}$ . (The notation and development here follow that of Percival and Walden [2000], to which we refer the reader for a full development of results summarized here.) Then, for a wide class of data series (including detrended density profiles),  $\mathbf{X}$  can be expressed as the sum of a (vector) “smooth part,”  $\tilde{\mathbf{S}}_{J_0}$ , and (vector) “details,”  $\tilde{\mathbf{D}}_j$ ,  $j = 1, 2, \dots, J_0$ :

$$\mathbf{X} = \sum_{j=1}^{J_0} \tilde{\mathbf{D}}_j + \tilde{\mathbf{S}}_{J_0}. \quad (1)$$

$\tilde{\mathbf{S}}_{J_0}$  consists only of variations in  $\mathbf{X}$  on scales  $2^{J_0}\delta$  and longer, while the  $\tilde{\mathbf{D}}_j$  vary, respectively, on scales  $\tau_j = 2^{(j-1)}\delta$ . Moreover, because we use a zero-phase wavelet filter, the details associated with a given scale take on large amplitudes at only those locations where the original data series  $\mathbf{X}$  displays large variations on the same scale; this will allow us to see, for example, whether strong variations on short scales occur at seasonal density transitions in our series. Equation (1) constitutes a multiresolution analysis, i.e., a series of pictures of how the data series “looks” on different scales.

The details and the smooth part are derived from vectors  $\tilde{\mathbf{W}}_j$ ,  $j = 1, 2, \dots, J_0$ , and  $\tilde{\mathbf{V}}_{J_0}$ , which are in turn computed recursively (one scale from another), and

component by component, from the original data series and filter coefficients (which are specific to the choice of wavelet),  $\tilde{h}_{j,l}$ ,  $\tilde{g}_{j,l}$ ,  $l = 0, 1, \dots, L-1$  [see Percival and Walden, 2000, section 5.3].

$$\tilde{W}_{j,t} \equiv \sum_{l=0}^{L_j-1} \tilde{h}_{j,l} X_{t-l_{\text{mod}N}} \quad \text{and} \quad (2)$$

$$\tilde{V}_{j,t} \equiv \sum_{l=0}^{L_j-1} \tilde{g}_{j,l} X_{t-l_{\text{mod}N}}$$

where  $t = 0, 1, \dots, N-1$  is the  $t$ -th component of the corresponding vector, and where  $L_j \equiv (2^j - 1)(L - 1) + 1$ . The  $\tilde{W}_j$  characterize variations on scales  $\tau_j = 2^{(j-1)}\delta$ , and  $\tilde{V}_{j_0}$  involves only variation on scales  $2^{j_0}$  and longer. They are useful not only as intermediaries in constructing details and the smooth part but also because they provide an analysis of variance of the original data series; that is, they provide a decomposition of the total variance in the data series,  $\hat{\sigma}_{\mathbf{X}}^2$ , into variances due to variations on distinct scales,  $\tau_j$ :

$$\sum_{j=1}^{J_0} \frac{1}{N} \|\tilde{W}_j\|^2 + \frac{1}{N} (\|\tilde{V}_{j_0}\|^2 - \bar{\mathbf{X}}) = \hat{\sigma}_{\mathbf{X}}^2, \quad (3)$$

where the square of the length of a vector  $\mathbf{A}$  (representing either  $\tilde{W}_j$  or  $\tilde{V}_{j_0}$ ) is given by  $\|\mathbf{A}\|^2 = \mathbf{A}^T \mathbf{A}$ , and  $\bar{\mathbf{X}}$  denotes the mean of the components of  $\mathbf{X}$ . The set of  $\frac{1}{N} \|\tilde{W}_j\|^2 \equiv P_W(\tau_j)$  is called the empirical wavelet power spectrum; when plotted as a function of  $\tau_j$ ,  $j = 0, 1, \dots, J_0 - 1$ , this spectrum provides an estimate of the variance in  $\mathbf{X}$  as a function of scale.

Note, however, that the circular filtering indicated in equation (2) implies that some elements of each  $\tilde{W}_j$  depend on combinations of data points from the beginning and the end of the data series. In general, this leads to a statistical bias in the sample  $P_W(\tau_j)$  as estimators for the true wavelet power spectral coefficients [Percival and Walden, 2000, chapter 8]. Elimination of the bias requires foregoing the use of components of  $\tilde{W}_j$  that depend on circular extension of the original series, with a corresponding loss of wavelet power spectrum estimates at the longest scales in the data. We have compared biased and unbiased estimates for  $P_W(\tau_j)$  in all of our data series and find that differences are typically minor for these particular series. Because density variations on the longer scales are important to the overall picture of density stratigraphy, we employ the potentially biased wavelet power spectrum estimates in our detailed analysis of selected firn density profiles in the section 2.3.1. In section 2.4, however, we focus on fine-scale density variance only and therefore employ only unbiased estimates of  $P_W(2 \text{ cm})$ .

### 2.3. Detailed Analysis of Representative Firn Density Profiles

Examination and assessment of both seasonal and fine-scale density variations requires detailed analysis of many firn density profiles. We have performed such analyses on all 12 of the density series described above and base our conclusions about the importance of variations on different scales on this full set of analyses. We find, however, that similar qualitative characteristics of seasonal and fine-scale density variations are common

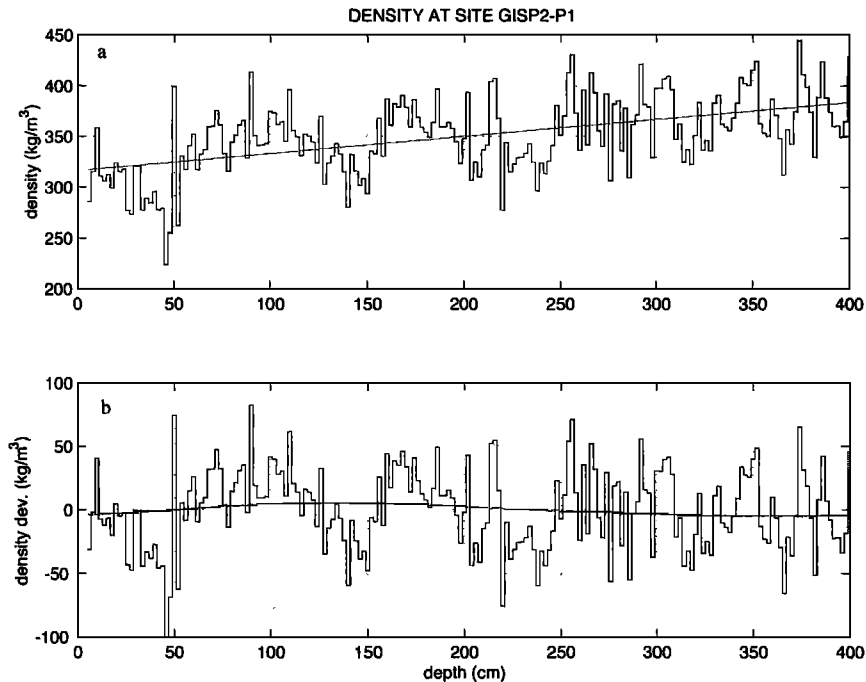


**Figure 1.** Four-meter long density profiles with 2-cm resolution at the first pit dug near the GISP-2 site in 1998: (a) raw density data and a linear fit to the data, (b) detrended series together with the wavelet smooth of order  $J_0 = 6$  (smooth line) in its wavelet decomposition.

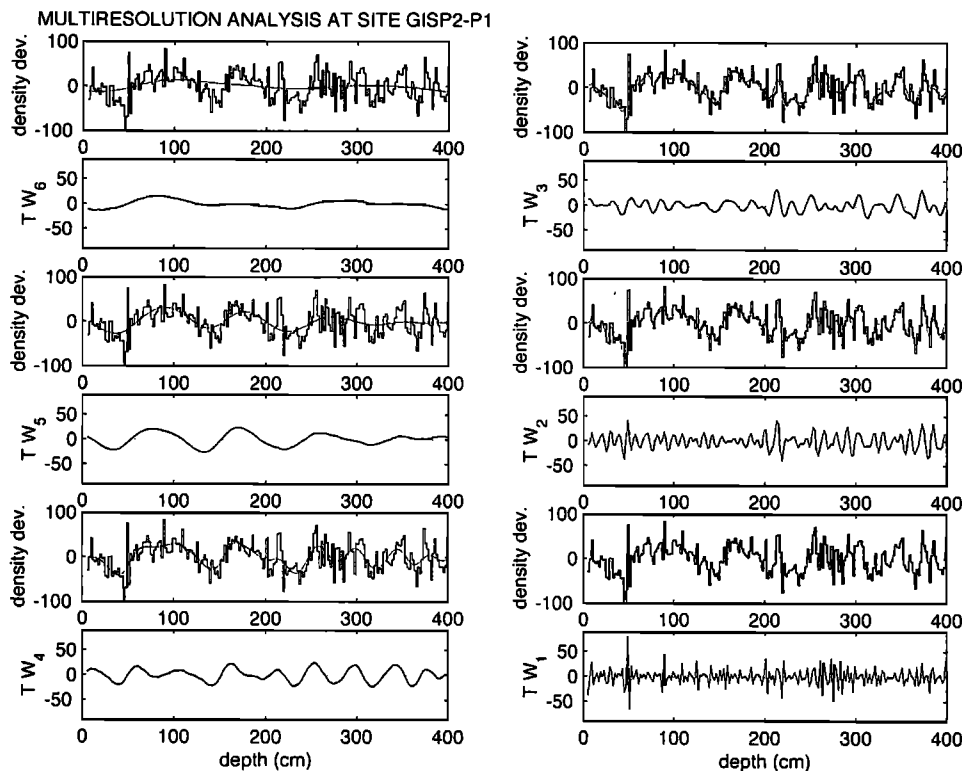


**Figure 2.** A wavelet multiresolution analysis of the data in Figure 1. Proceeding first down the left column, and then the right, the analysis is presented in vertical pairs of plots which display the effect of including progressively finer scales. The top plot in each pair shows the detrended density data and the sum of the wavelet smooth plus details, up to the order indicated by the label of the wavelet coefficient in the bottom plot. Thus the plot in the top left shows (as a smooth line) the sum of the wavelet smooth of order  $J_0 = 6$  and the detail corresponding to variations on scales  $J_0 - 1$ , that is,  $2^5 \delta = 64$  cm. The plot immediately beneath shows the 64-cm-scale wavelet coefficient aligned with the density series, from which it can be seen where in the depth record variations at 64-cm scale are appreciable. The next pair adds variations on 32-cm scale to the wavelet reconstruction, and so on to the pair in the bottom right, which shows the completely reconstructed density series (the wavelet smooth plus all details) and the finest-scale (2 cm) wavelet coefficients as a function of depth.

to all 12 series and to additional 2-cm-resolution density records as well that we have examined but (for a variety of reasons) not included in this report. For brevity, we therefore present here the full multiresolution analyses for four representative examples of the 12 series, namely, the series with highest and lowest accumulation rates, the longest data record, and an independent record nearly coincident in space and time with the longest record, to serve as an indicator of consistency.

### 2.3.1. Pits 1 and 2 at the GISP-2 site in 1998.

Figure 1 shows the longest data record in our set, a 4-m profile acquired roughly a kilometer from the GISP-2 ice core site. As is typical [Benson, 1971], the mean density increases with depth and, between zero and 4-m depth, the trend is linear to a good approximation (as shown by the linear fit to the data in Figure 1a). Figure 1b shows the density series with this linear trend removed, together with the wavelet smooth of order  $J_0 = 6$ , i.e., that component of the series that varies only on scales

$2^6 \times 2$  cm = 128 cm and longer. The seasonal variation of density, with firn originating in summer relatively less dense than that originating in winter [Benson, 1971; Alley, 1988], is readily apparent in both plots; the accumulation rate at this site ( $265 \text{ kg m}^{-3} \text{ yr}^{-1}$ ) puts that variation on scales of decimeters to a meter (as will be seen more precisely momentarily). A careful reading of the stratigraphy, confirmed by stable isotope analysis, indicates that this density record samples deposition at times reaching back to the winter of 1991–2. This record thus overlaps two other records in our study: pit 2 at the GISP-2 site in 1998, a 2-m record which sampled a period of accumulation higher than the 1994–1998 average, and the 2-m GISP-2 record acquired in 1995, which sampled a period of accumulation lower than the average.

Note that with the possible exception of the most recent winter/spring transition in the record (at about 50-cm depth), the seasonal transitions in the density record are gradual, with scales of at least 10 cm. Equally

prominent are density variations on scales of decimeters down to the resolution limit of 2 cm, which have certainly been observed many times before, though less vividly, in 5-cm-resolution data [Benson, 1971; Alley, 1988; West *et al.*, 1996]. The intensity of fine-scale variation does not notably vary between strata from winter versus summer. Neither is there any obvious depth variation in fine-scale stratification, though (see below) the 2-cm-scale variance estimate for this 4-m record does turn out to fall between those from the 2-m GISP-2 series from 1998 (high accumulation rate) and 1995 (low accumulation rate).

Figure 2 shows a multiresolution analysis of the GISP-2 pit-1 record. We progressively add finer-scale wavelet details to the smooth part and, at each step, plot the wavelet coefficients for that scale (translated so as to align them with the original series) to show where, in depth, large variance on that scale occurs. The sum of the smooth part plus details on scales of 64, 32, and 16 cm reproduces the seasonal variation in the series. The short-scale “noise” within seasonal transitions does not obviously differ from that in the middle of seasons (which is consistent with the result of the stationarity test). From the plot of the wavelet coefficient for 2-cm scales, it is clear that density (and thus permittivity) variations on scales fine enough to affect emission are not particularly associated with seasonal transitions in this record; what appears to be a crust/hoar layer couplet at the boundary of the uppermost spring transition is the only coincidence out of eight possibilities (and even that event fails to appear in the second GISP-2 record from 1998; see below).

The empirical wavelet power spectrum in Figure 3 shows a broad relative maximum at scales of 16 and 32 cm and a relative minimum at a scale of 8 cm. (The estimates plotted in this instance are the potentially biased estimates, as explained in section 2.2.) The variance due to the annual cycle of seasonal density variations in Figure 1 separates in scale, for this accumulation rate, from the variance on other scales. Data from the other sites confirm and expand this view, and we will return to discuss its implications in the following subsection. Perhaps most striking, however, is the proportion of total variance accounted for by variations on the shortest scales: the variance on 2-cm scales alone accounts for nearly a third of the total, and the sum of variances on 2- and 4-cm scales accounts for more than half.

These characteristics of the near-surface firn at the GISP-2 site in 1998 are confirmed by the second density series, which was acquired approximately 2 km away and 9 days after the first, and shown together with its wavelet power spectrum in Figure 4. In this case, all of the seasonal transitions, including the most recent winter/spring transition, are gradual on the scale of a 4.5-cm wavelength. The empirical wavelet power spectrum for this site (Figure 4b) shows a peak due to annual density variation similar to the first record but slightly lower variance at fine scales. This differ-

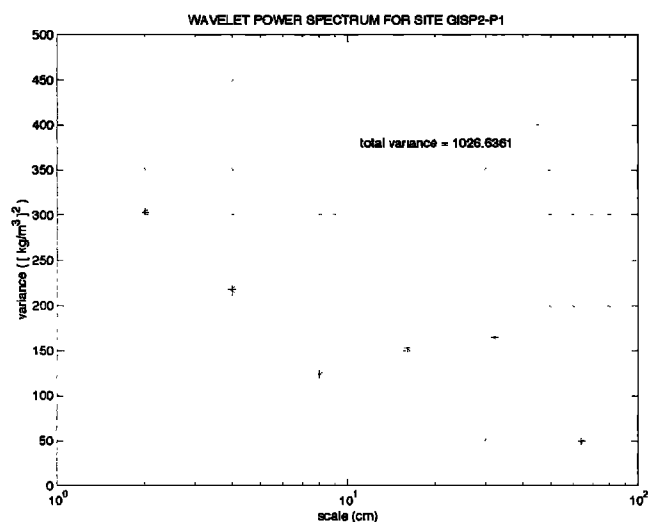


**Figure 3.** Semilog plot of the empirical wavelet power spectrum for the data in Figure 1, based on potentially biased estimates (see section 2.2).

ence appears to be associated with temporal variability in accumulation rate, with higher accumulation in the few years prior to 1998 than earlier. Indeed, stable isotope analysis of the 1995 profile from the GISP-2 site [Shuman *et al.*, 1998] indicates an accumulation rate of only  $191 \text{ kg m}^{-3} \text{ yr}^{-1}$  between approximately mid-1992 and mid-1995, and this lower accumulation rate is apparently associated with a somewhat higher density variance on the 2-cm scale (see Figure 9 and Table 1, though note the uncertainty implied by results from the Kenton and GRIP sites).

**2.3.2. Southwest (high accumulation) site in 1998.** By contrast the highest accumulation site in our data set, 60 km southwest of Summit, clearly shows fewer annual cycles in its 2-m depth (see Figure 5). The multiresolution analysis for this record shows very gradual seasonal transitions in all cases. The (potentially biased) wavelet power spectrum estimates (Figure 6) clearly show the annual cycle at the 32-cm scale. Most notable, however, are the very low 2- and 4-cm variances in this record; this is the only case in our data set where those variances do not account for more than half the total in the record.

**2.3.3. Antarctic F (lowest accumulation) site in 1996.** Figure 7 shows the density profile and multiresolution analysis from the lowest accumulation rate site in our data set, site F, near Siple Dome in West Antarctica. Accumulation at this site was roughly 22% of that at the Southwest site in Greenland. Fine-scale density variation in this record is very large and appears nearly to dominate annual density variations. The multiresolution analysis suggests that the sum of details down to 8-cm resolution may track the seasonal variation; this suggestion is supported by the plot of (potentially biased) wavelet power spectrum estimates in Figure 8. Inspection of the fine-scale wavelet coefficients,

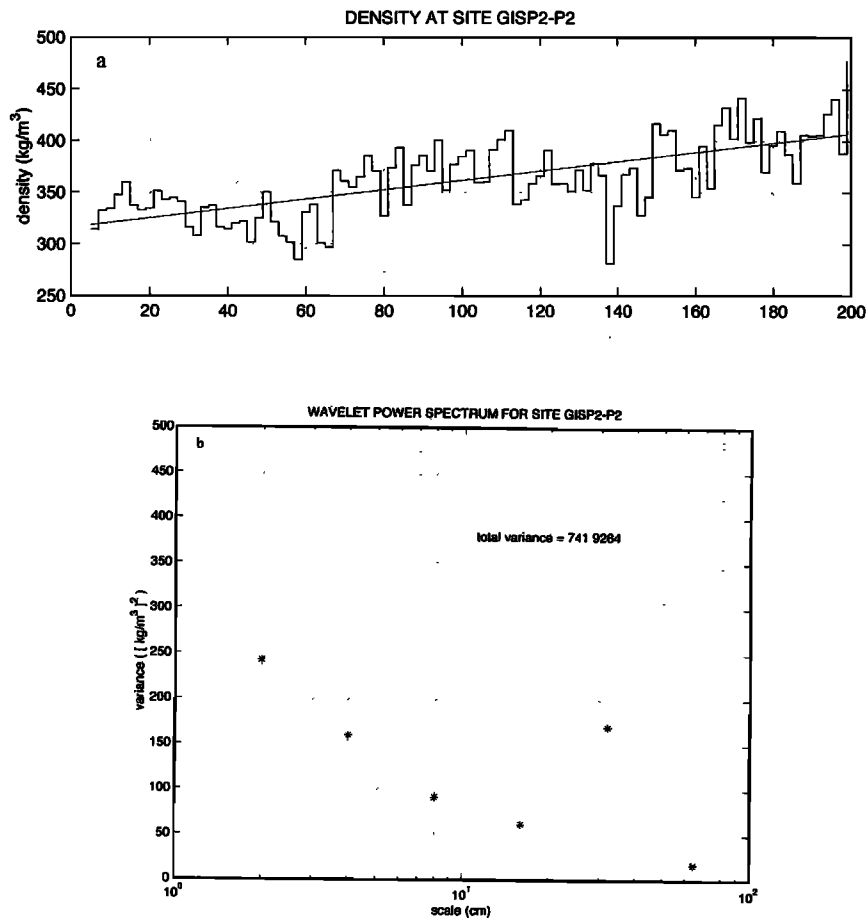


**Figure 4.** A 2-m-long density profile with 2-cm resolution at the second pit dug near the GISP-2 site in 1998: (a) raw density data and a linear fit to the data, (b) semilog plot of the empirical wavelet power spectrum for the data in Figure 4a.

however, shows no evidence that abrupt changes in density are particularly associated with putative seasonal variations. Thus none of the records in section 2.3 show much evidence for seasonal transitions that are sharp on 2- to 4-cm scales.

#### 2.4. Fine-Scale Variance Versus Accumulation Rate

Variance at 2- and 4-cm scales (the scales most significant for emission at 4.5-cm wavelength) could, in principle, arise from sharp density transitions at seasonal boundaries, from nonseasonal weathering, or both. However, neither the data analyses presented above nor those of the other eight data series yield any evidence for consistently sharp transitions at seasonal boundaries.

Neither do those analyses support the scenario of centimeter-scale layers with mean thicknesses that vary linearly with accumulation rate. The data do illuminate the likely cause of the earlier inference of such layers, however. The previous studies of *West et al.* [1996], *Arthern et al.* [1997], and *Winebrenner and Arthern* [1998] based on 5-cm-resolution data and classical spectral analysis involved a Nyquist frequency of approximately 10 cm in depth and density records from areas

with accumulation rates mostly similar to those in this study. Thus the finest-scale variation that the earlier analyses sampled was that on scales corresponding to the annual cycle of density, i.e., variation tied directly to the annual accumulation rate. Moreover, the earlier work relied on fitting an assumed spectral form to spectral estimates from the data such that a smaller (larger) accumulation rate, and thus more (less) variance at shorter depth scales, was interpreted as a smaller mean thickness of homogeneous layers on the order of a few centimeters. Thus the reason for the apparent covariance of centimeter-scale layer thicknesses with accumulation rate is now clear, though its interpretation was clearly mistaken. Resolution of that issue leaves open, however, the physical cause of the observed relationship between 4.5-cm emission (specifically, polarization) and accumulation.

Our fine-resolution data suggest an alternative explanation. Figure 9 shows statistically unbiased (compare section 2.2) estimates of the wavelet power spectrum on the 2-cm scale versus accumulation rate for our 12 sites. We also denote 67% ("1 $\sigma$ ") confidence limits on the power spectrum estimates, which we compute using the simplest (and most robust, though possibly pessimistic)

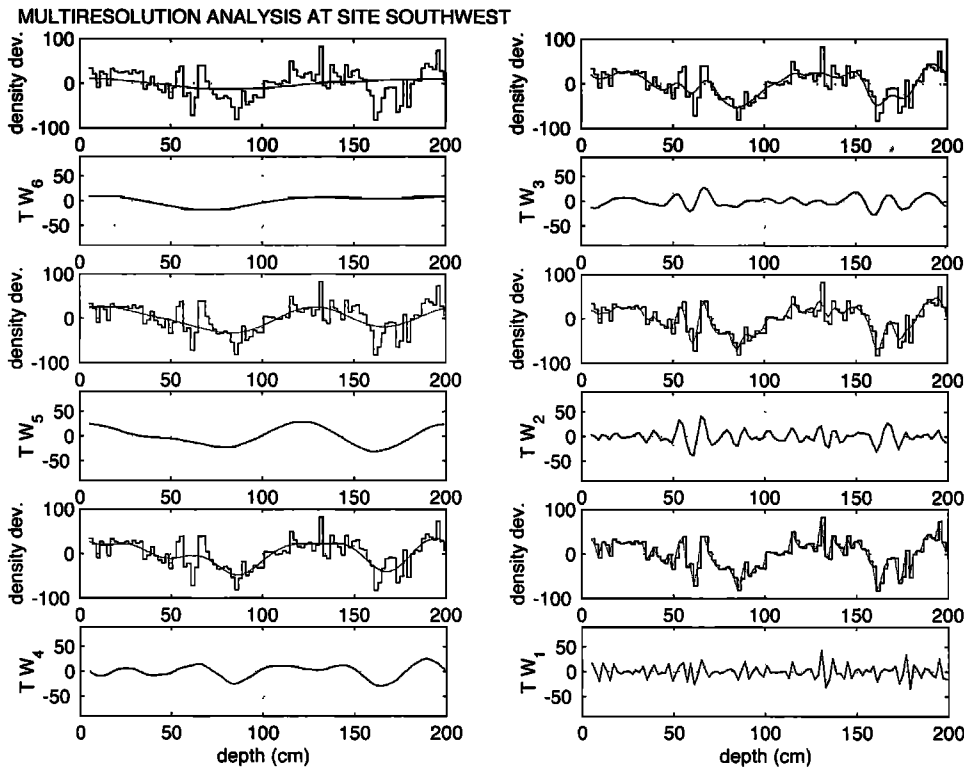


**Figure 5.** Multiresolution analysis of a 2-m-long density profile with 2-cm resolution from a pit dug approximately 60 km southwest of the GISP-2 site in 1998. Presentation is the same as that in Figure 2.

method given by *Percival and Walden* [2000] (see their section 8.4, equation (314c)). While the number of data points is not large, and their associated uncertainties are, it seems clear that there is a significant relationship between fine-scale density variance and accumulation rate. Note that even sub-decadal-scale temporal variability in accumulation rate at a single site is reflected in near-surface (0–2 m) fine-scale variance, as evidence by the data from GISP-2 in 1995 and 1998. The present data support no more than a linear fit, though extrapolation

of such a fit to accumulation rates larger than those in our data would predict zero 2-cm-scale variance at approximately  $350 \text{ kg m}^{-3} \text{ yr}^{-1}$ , which suggests to us that the true relationship is likely to be nonlinear. Thus the need for more data is clear, but in our view, this analysis strongly indicates a relationship of the type that would mediate the observed relationship between 4.5-cm emission and accumulation rate.

The physics responsible for this relationship seems likely to be intraseasonal weathering, including especially crust and hoar layer formation [*Alley, 1988; Goodwin, 1988*]. It has yet to be shown, however, whether modeling of snow weathering can quantitatively explain the observations and illuminate the relative importance of crusts and other features in that explanation. We have verified by computation that crusts with parameters similar to those observed [*Alley, 1988; Goodwin, 1988*] can be responsible for at most half of the 2-cm-scale variance we observe and much less than that of the observed 4-cm-scale variance. Thus both crusts and longer-scale firn density features must both contribute to our observations. Whether both must contribute to the radiometric behavior of firn at 4.5-cm emission is the subject of the following section.

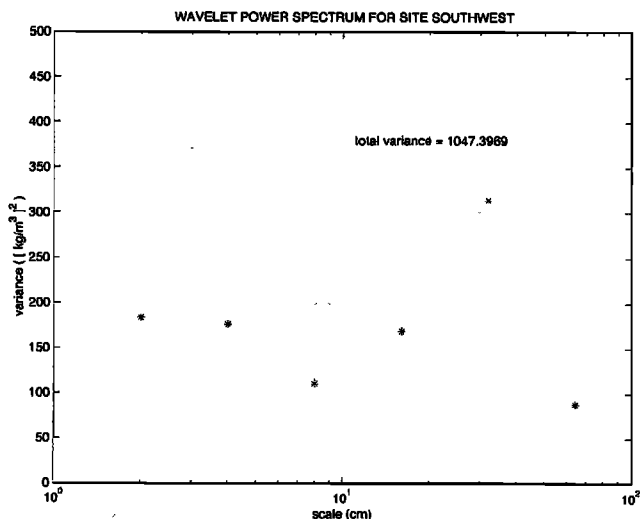


**Figure 6.** Semilog plot of the empirical wavelet power spectrum for the data in Figure 5.

### 3. Microwave Emission Through Fine-Scale Firn Stratification

The picture of firn that emerges from the previous section is that of a layered structure in which density,

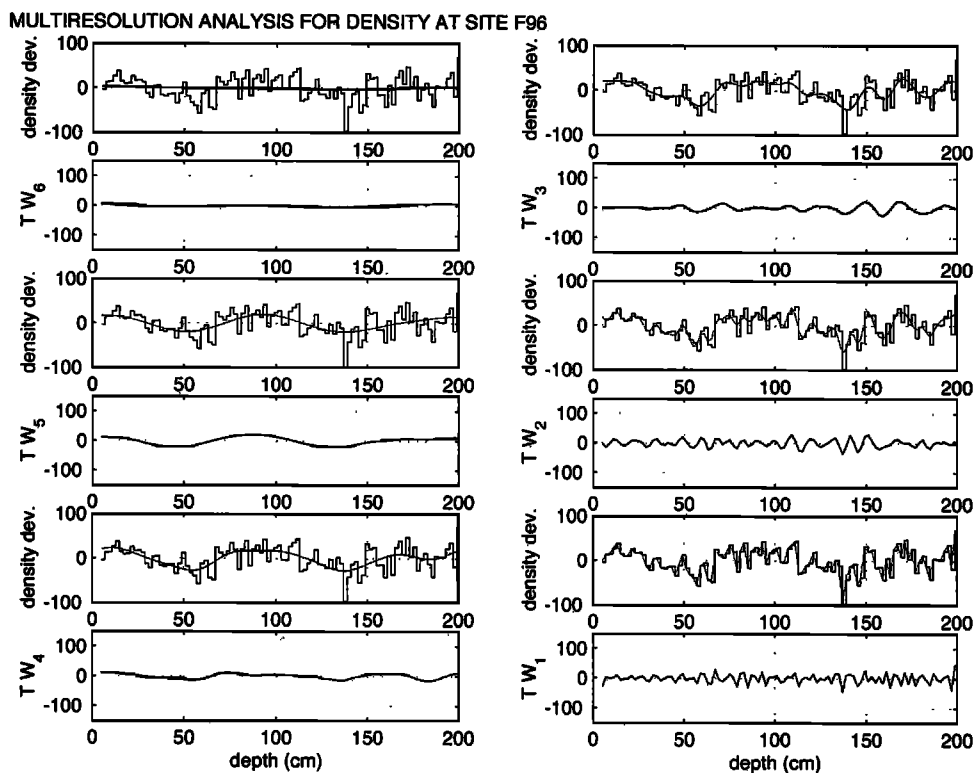


**Figure 7.** Multiresolution analysis of a 2-m-long density profile with 2-cm resolution from a pit dug at a low-accumulation site near Siple Dome, West Antarctica, in the austral spring of 1996. Presentation is the same as that in Figure 2.

and thus the effective permittivity pertinent to 3- to 6-cm microwave emission, vary significantly on a variety of scales in the upper few meters of firn. The important scales for microwave emission are millimeter to centimeter scales, which account for more than half of the total variance in 2- to 4-m density records, and which are sufficiently short (compared to the wavelength) to cause significant reflection [Brekhovskikh and Godin,

1998; Surdyk and Fily, 1995]. The density and scale of firn crusts effectively guarantee their importance to 3- to 6-cm emission. The importance of low density, large-crystal hoar layers, as well as other centimeter-scale density variations, at 3–6 cm is less clear, but may well also be substantial (as they certainly are at shorter wavelengths [Surdyk and Fily, 1995; Abdalati and Stefan, 1998]).

Density profiles over depth ranges greater than those in our data show that fine-scale density variations decrease with increasing depth, because of equalizing effects of densification [Alley and Bentley, 1988]. The characteristic length scale of the decrease is roughly 6 m [Stephenson, 1970; Benson, 1971; Alley and Bentley, 1988]; the density contrast between crusts and surrounding firn may decrease on a depth scale as short as a few meters [Alley, 1988]. Seasonal temperature variation in near-surface firn is damped on a similar depth-scale [Paterson, 1994]. The length scale of absorption in firn at 3- to 6-cm wavelength, however, is on the order of 30 m [Mätzler, 1987; Rott et al., 1993].

Thermal emission at those wavelengths therefore originates predominantly from depths where the firn is relatively homogeneous in density and isothermal at its mean surface temperature. Energy emitted from the relatively thin depth range of strong layering and variable temperatures only slightly affects total emission, as is evidenced by the observation that 4.5-cm brightness

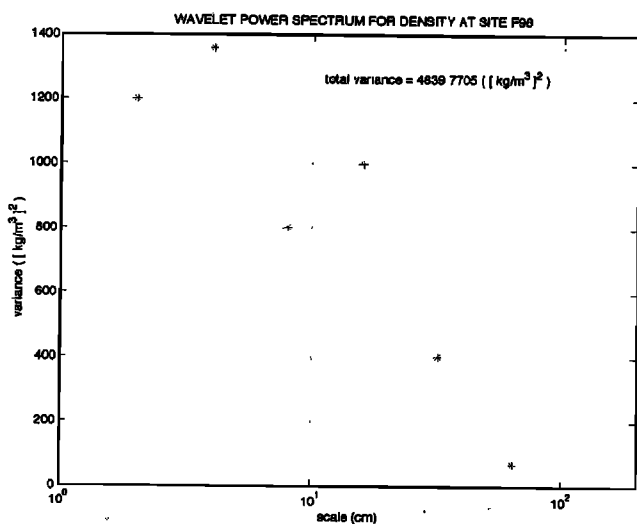


**Figure 8.** Semilog plot of the empirical wavelet power spectrum for the data in Figure 7.

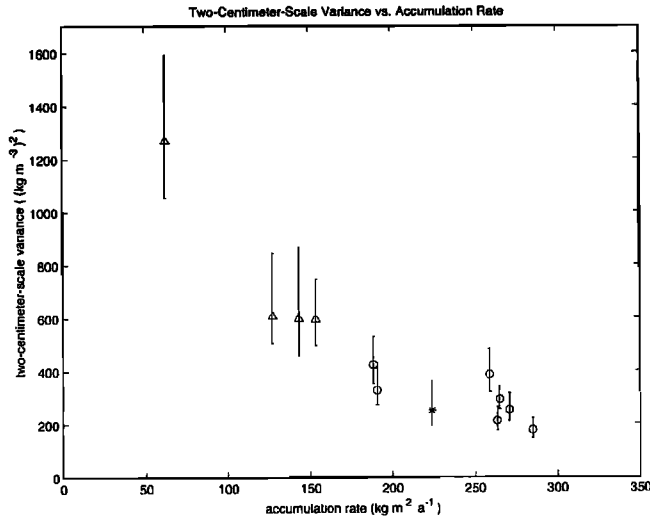


**Figure 9.** Plot of statistically unbiased estimates (see section 2.2) of the wavelet power spectrum on 2-cm scales (i.e.,  $P_w(\tau_1)$ ), versus accumulation rate for the seven Greenland sites (circles) and five Antarctic sites (triangles, except for G96 which is plotted with an asterisk because the accumulation rate estimate for that site is based on only 2 years of accumulation). The error bars denote 67% (“ $1\sigma$ ”) confidence limits on the wavelet power spectral estimates, based on *Percival and Walden* [2000, equation (314c), section 8.4]. Specific sites on this plot may be identified by reference to Table 1, where accumulation rates and unbiased 2-cm-scale variance estimates for each site are given numerically.

temperatures show seasonal dependences of no more than 2% [Rott, 1989; Zhang et al., 1989; Fily and Benoist, 1991]. For the same reason, however, nearly all of the emitted radiation must traverse the strong near-surface stratification. The reflecting properties of that stratification alter the radiative balance, and thus the emitted radiation, in a way that depends strongly on both polarization (for observation directions other than normal to the layering) and the fine-scale layering.

It is therefore a useful first approximation to model 3- to 6-cm firn emission as originating from an isothermal system (at the mean surface temperature) composed of dense, homogeneous firn, overlain by random millimeter- and centimeter-scale layering but neglecting layering on decimeter and longer scales. We idealize the actual layering as truly one-dimensional, but random, for purposes of Monte Carlo emission calculations. (Roughness of layer interfaces on meter scales and longer effectively produces averaging over layer configurations and is accounted for by our Monte Carlo procedure. Roughness on decimeter and shorter scales will tend to reduce polarization of emitted radiation slightly [Tsang et al., 1985], but we neglect this effect in this initial work.) Because our observations do not fully specify the fine-scale layering, but the importance of crusts to emission is clear, we provisionally model fine-scale layering in terms of two random components.

The first is composed of homogeneous centimeter-scale layers with independent random (gaussian distributed) densities and (exponentially distributed) thicknesses. We varied the mean thickness linearly with accumulation rate and set the variance of layer density according to the earlier relations of *Arthern et al.* [1997] because, despite the mistaken interpretation that originally produced them, those relations help layering in the present model to reproduce (approximately) the variation of 2- and 4-cm-scale variance we now observe. They may also mimic the actual layers resulting from hoar formation and other weathering. The centimeter-scale variance is tapered at depths between 5 and 15 m in a fashion similar to that in the model of *West et al.* [1996]. The second layering component is millimeter-scale firn crusts, also independently random in thickness with an exponential distribution and mean 0.6 mm, with densities set by reference to (sparse) ground observations [Alley, 1988; Goodwin, 1988], and with a fixed, independent probability of occurrence at any layer interface generated by the first component. This probability, together with the linear dependence of mean centimeter-scale layer thickness on accumulation rate, determines a mean number of crusts per year of snow accumulation in our stratification model.

We compute for this firn model the average emission at 4.5-cm wavelength, and an observation angle of  $50^\circ$  (corresponding to the observation angle of the sensor we employ; see below), by generating several thousand realizations and averaging emissivities (for each choice of parameters). We then compute a standard measure of the polarization of emission, the so-called polarization ratio,

$$P = \frac{e_v - e_h}{e_v + e_h} \approx \frac{T_v - T_h}{T_v + T_h}, \quad (4)$$

where  $e_v$  and  $e_h$  are vertically and horizontally polarized emissivities, and  $T_v$  and  $T_h$  are vertically and horizontally polarized brightness temperatures, all at  $50^\circ$  observation angle. When computed from observations, this quantity constitutes a signature approximately independent of physical temperature (to first order, except near the melting temperature).

Figure 10 shows results of four simulations of  $P$  as a function of accumulation rate  $A$ , with differing assumptions for poorly known crust parameters. Curve a is the result when the layering model includes centimeter scale alone, with no crusts. Curve b results by assuming a crust density of  $650 \text{ kg m}^{-3} \text{ yr}^{-1}$  and probability of occurrence at centimeter-scale layer interfaces of 0.6. Curve c results by assuming a crust density of  $690 \text{ kg m}^{-3} \text{ a}^{-1}$  and occurrence probability 0.6, and curve d by assuming a density of  $690 \text{ kg m}^{-3} \text{ yr}^{-1}$  and occurrence probability 1.0 (a crust at every centimeter-scale layer interface). The occurrence probability of 0.6 produces a crust frequency in the model of approximately seven crusts per year, on average.

According to these results, observable polarization can result from centimeter-scale layering alone, but

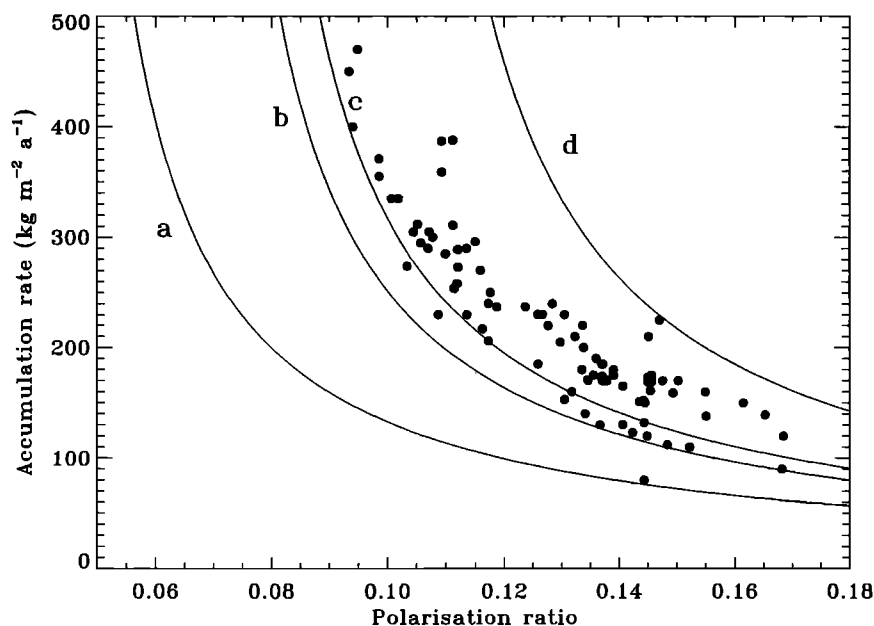


**Figure 10.** A plot of accumulation rates versus polarization ratios for emission at 4.5-cm wavelength and  $50^\circ$  incidence angle, both theoretical and observed. The observed polarization ratios are from SMMR data from 1979 to 1985. The observed accumulation rates are from ground data compiled by *Ohmura and Reeh* [1991]. The four theoretical curves result from the model and parameter choices described in the text and represent the effects of increasing crust density and frequency going from curve a to curve d.

crust-induced polarization seems likely to figure strongly in the theoretical polarization/accumulation rate relationship.

For comparison, Figure 10 also shows accumulation rates and polarization ratios at locations of ground observations of accumulation rate in the dry snow zone, which were acquired between roughly 1912 and 1986 and compiled by *Ohmura and Reeh* [1991]. The locations are indicated by cross marks in the map shown in Plate 1. We estimated polarization ratios at those locations using brightness temperature observations from the gridded Scanning Multichannel Microwave Radiometer (SMMR) data set produced by the NASA Goddard Space Flight Center [*Gloersen et al.*, 1992]. Specifically, we averaged brightness temperatures pixel-wise for all of Greenland between October 1979 and December 1985 to produce brightness temperature maps of nominally 25-km resolution. (Although the underlying resolution of the 4.5-cm data is roughly 150 km, the interpolation onto a 25-km grid inherent in the gridded data appears to usefully depict smoothed but probably real features in the underlying brightness temperature fields.) We next adjusted average vertically polarized brightness temperatures upward by 6 K to bring observed values in seasonally melting zones in summer into agreement with those expected on the basis of ground observations of wet snow emission. (While this procedure hardly constitutes a proper calibration correction, it is a provisional means to address what appears to be a local calibration offset, pending re-examination using the recent Pathfinder reprocessing of the SMMR data.

Even without the procedure, the results in Figure 10 would be altered only in that they would seem to show slightly less influence of crusts.) Finally, from the average brightness temperatures, we computed  $P$  pixel-wise and selected those pixels containing the locations in the *Ohmura and Reeh* [1991] compilation.

The form of the observed relationship between polarization and accumulation is, in our view, strikingly similar to that predicted by our physical model (all the more so given the uncertainties in point accumulation rate observations spread over a period of decades). One of our sets of parameter choices specified from independent ground data (curve c) yields nearly a fit to the observations. Moreover, most of the variation in observed polarization in Figure 10 is due to variation in horizontally polarized emission, with lower emission corresponding to larger polarization; this correspondence is precisely opposite to what would be expected if emissivity variations were controlled by scattering from ice grains [*Tsang et al.*, 1985], but is expected for a stratification-reflection mechanism because the SMMR observation angle ( $50.3^\circ$ ) is close to the Brewster angle for a material with the effective permittivity of near-surface firn ( $\approx 53^\circ$ ). Thus, in our view, the evidence is strong that fine-scale density stratification is the dominant control on Greenland firn emission near  $50^\circ$  observation angle and 4.5-cm wavelength and that variations in that stratification as a function of accumulation rate, perhaps crust spacing in particular, link accumulation rate to the polarization of emission.

The observations and theory for snow weathering

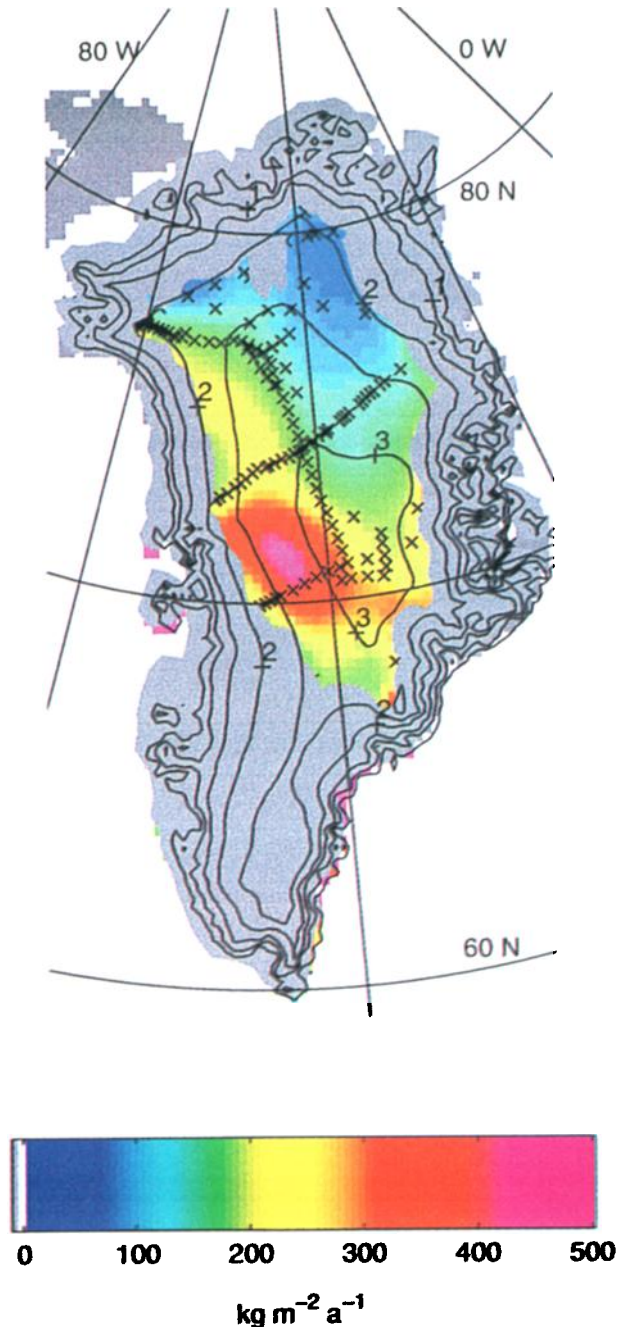


**Plate 1.** A map of the accumulation rate field in the dry snow zone of Greenland, based on 4.5-cm-wavelength SMMR observations from 1979 to 1985 and the relationship between the polarization of emission at the wavelength and accumulation rate shown by curve c in Figure 10. Areas of seasonal melting are masked in grey based on the observations of *Mote and Anderson* [1995]. Crosses mark the locations of ground observations of accumulation rate compiled by *Ohmura and Reeh* [1991]. The contours show elevation in kilometers and are from the digital elevation model of Greenland produced by *Ekholm* [1996].

presently available (to us) do not, however, definitively, testably specify the stratification/accumulation linkage; neither do we yet know the conditions under which that linkage may change or fail. Use of any curve in Figure

10 (whether fit to data or not) as the basis for mapping accumulation rate therefore remains, at this juncture, empirical in an essential way. However, we think that provisional use of such a curve to translate observed polarization into an accumulation rate field nonetheless provides both a new check on our understanding by comparison with additional known accumulation rates and may show putative new features in the accumulation rate field that merit investigation. We therefore undertake accumulation rate mapping based on curve c in Figure 10, the nearest match between independently specified theory and observation, in section 4.

#### 4. Accumulation Rate Mapping

We produced a putative accumulation rate map from the average brightness temperature maps described in section 3 by simply computing  $P$  at each pixel. We did not smooth or otherwise try to reconcile neighboring pixel values (any smoothing in our map results solely from whatever smoothing was introduced by the gridding process used to produce the underlying data). We next used curve c in Figure 10 to assign an accumulation rate to each pixel value of  $P$ . Because curve c runs slightly below the observations, we expect this provisional accumulation rate map to be biased slightly low, especially at the lowest accumulation rates, where the bias may exceed 15% (the price for refraining from a simple curve fit). Finally, we have masked those parts of Greenland that were observed to melt seasonally by *Mote and Anderson* [1995], since those regions include snow and ice structures which are very different from those in dry snow zones and to which our theory does not apply. Plate 1 shows the result of this process, together with the locations of ground observations compiled by *Ohmura and Reeh* [1991] and contours of surface elevation from the digital elevation map of Greenland produced by *Ekholm* [1996].

The large-scale pattern shown in Plate 1 agrees broadly with the map synthesized by *Ohmura and Reeh* [1991] as well as with earlier syntheses; the accumulation regime changes rapidly across the central ridge of Greenland, with high rates to the south and especially southwest and low rates to the north. However, the spatial distribution of ground data that specify the polarization/accumulation rate relationship span all the major accumulation regimes in Greenland. The broad agreement may therefore indicate only that neighborhoods of the ground data locations are similar in both accumulation rate and polarization ratio.

More interesting, in our view, are the very high accumulation area to the southwest of Summit and the tongue of high accumulation reaching upslope from southeast to just south of Summit. The southwest feature appears on the map of *Ohmura and Reeh* [1991], though in a significantly different shape, and is not obviously associated with topography. The challenge this feature presents to ice sheet precipitation modeling, because it evidently results from a subtle interplay

of topography and meteorology, [Chen and Bromwich, 1999] motivates testing of the shape we predict. In contrast, the south/southeast accumulation tongue appears, *prima facie*, to be associated with a draw extending to the southeast, and it does not appear fully in earlier accumulation maps. Note that none of the ground data in Figure 10 sample this feature; the feature is therefore an independent prediction of our mapping technique and should be interesting to test against new ground observations. Finally, we note that the indication on our map of a decrease in rates toward the southernmost part of the unmasked area may be an indication that seasonal melting had occurred there in roughly the decade preceding the SMMR observations (though not in the period studied by Mote and Anderson [1995]); melting would introduce low-porosity ice layers in the upper few meters of firn, increasing polarization by a mechanism not in the model on which we base our map, and skewing our accumulation rate retrieval. Alternatively, the problem might arise because the spatial resolution of the underlying emission observations is coarse; this could "smear" the brightness temperature boundaries between melting and nonmelting zones and introduce anomalously large polarization ratios where the melt mask correctly indicates perennially dry snow.

The timescale on which the upper few meters of firn accumulates is roughly the temporal averaging period prior to observation for our accumulation rate retrievals. Thus in high accumulation rate areas, our method averages over a fraction of decade, and we expect that emission observations may be used to observe decadal-scale accumulation variations. In low accumulation regions, however, the firn responsible for the signature we observe requires many decades to accumulate, and we expect that our retrievals thus constitute long-term averages in those regions. The first look at any changes in 4.5-cm emission from the ice sheets since the SMMR period, and thus indications of decadal accumulation rate variability, will be provided by observations from the two Advanced Microwave Scanning Radiometer (AMSR) instruments due for launch in the near future.

## 5. Conclusions

Our analysis of variance versus depth scale in firn density profiles reveals that a large fraction of the total variance is due to stratification on scales of a few centimeters and shorter. The glimpse of a relation between fine-scale variance and accumulation rate is a consequential outcome of our analysis, but is surely still partial and must be expanded by analysis of a larger body of existing data and, we hope, new observations designed specifically for the purpose. Moreover, the physics leading to observed fine-scale stratification remain quantitatively indeterminate, but this study makes clear the prospective value of a quantitative theory of fine-scale firn weathering.

A key application of that basic study will be, according to our modeling and observations, a fully physically based method of mapping accumulation rate fields using satellite-based observations of ice sheet emission. At present, our emission model based mostly on crust characteristics, especially depth spacing as a function of accumulation rate, is consistent with our density observations, though not uniquely so. In addition to more purpose-designed field measurements and modeling, progress may come from combined analysis of emission observations at 4.5- and 2.8-cm wavelength. Based on preliminary computations, we expect differences between emission at those wavelengths to illuminate the roles of crusts versus centimeter-scale density variance because of greater dispersion in reflections caused by the latter. The two AMSR instruments will soon provide the first highly reliable set of dual-wavelength observations. Even with the present uncertainties and provisional inferences, however, we find it interesting to note the resemblance between the physical picture of firn emission at which we now arrive and that put forward nearly 30 years ago by Gurvich and coworkers [Gurvich *et al.*, 1973; Gurvich and Krasil'nikova, 1977].

Finally, our provisional map of accumulation rates in the dry snow zone of Greenland, while agreeing broadly with ground observations, makes specific, testable predictions in locations that are interesting geophysically. We think that tests of those predictions against ground observation, and intercomparison with precipitation modeling, will shed light on the physics of accumulation rate retrieval from satellite data as well on the accumulation rate fields themselves.

**Acknowledgments.** We would like to thank R.B. Alley, C.S. Benson, and H.J. Zwally for numerous valuable discussions and for their separate emphases of the characteristics and importance of firn crusts. We also thank T.L. Mote and M.R. Anderson for the provision of their Greenland melt data used to construct our accumulation rate map, S. Ekholm for provision of his elevation model for Greenland in digital form for comparison, and D.B. Percival for computations of confidence limits and several helpful consultations. Finally, we thank two anonymous reviewers whose comments led to significant improvements in the paper. This work was sponsored by NASA grant NAGW5-6819.

## References

- Abdalati, W., and K. Steffen, Accumulation and hoar effects on microwave emission on the Greenland ice-sheet dry-snow zones, *J. Glaciol.*, *44*, 523–531, 1998.
- Alley, R.B., Texture of polar firn for remote sensing, *Ann. Glaciol.*, *9*, 1–4, 1987.
- Alley, R.B., Concerning the deposition and diagenesis of strata in polar firn, *J. Glaciol.*, *34*, 283–290, 1988.
- Alley, R.B., and C.R. Bentley, Ice-core analysis on the Siple Coast of West Antarctica, *J. Glaciol.*, *11*, 1–7, 1988.
- Arthern, R.J., D.P. Winebrenner, and V. Wismann, Ice sheet accumulation rate estimates over Greenland from observations of microwave backscattering and emission (abstract), *Eos Trans. AGU*, *78*(46), Fall Meet. Suppl., F16, 1997.
- Bamber, J.L., D.G. Vaughan, and I. Joughin, Widespread

- complex flow in the interior of the Antarctic Ice Sheet, *Science*, **287**, 1248–1250, 2000.
- Benson, C.S., Stratigraphic studies in the snow at Byrd Station, Antarctica, compared with similar studies in Greenland, in *Antarctic Snow and Ice Studies II*, edited by A.P. Crary, pp. 333–354, AGU, Washington, D. C., 1971.
- Brekhovskikh, L.M., and O.A. Godin, *Acoustics of Layered Media I*, 242 pp., Springer-Verlag, New York, 1998.
- Chen, Q.-S., and D.H. Bromwich, An equivalent isobaric geopotential height and its application to synoptic analysis and generalized omega-equation in sigma-coordinates, *Mon. Weather Rev.*, **127**, 145–172, 1999.
- Clausen, H.B., N.S. Gunderstrup, S.J. Johnsen, R. Bind-schadler, and J. Zwally, Glaciological investigations in the Crête area, central Greenland: A search for a new deep-drilling site, *Ann. Glaciol.*, **10**, 10–15, 1988.
- Drinkwater, M.R., D.G. Long, and A.W. Bingham, Greenland snow accumulation estimates from satellite radar scatterometer data, *J. Geophys. Res.*, this issue.
- Ekhholm, S., A full coverage, high-resolution, topographic model of Greenland computed from a variety of digital elevation data, *J. Geophys. Res.*, **101**, 21,961–21,972, 1996.
- Fily, M., and J.-P. Benoist, Large-scale statistical study of Scanning Multichannel Microwave Radiometer (SMMR) data over Antarctica, *J. Glaciol.*, **37**, 129–139, 1991.
- Forster, R.R., K.C. Jezek, J. Bolzan, F. Baumgartner, and S. Gogineni, Relationships between radar backscatter and accumulation rate on the Greenland ice sheet, *Int. J. Remote Sens.*, **20**, 3131–3147, 1999.
- Gloersen, P., W.J. Campbell, D.J. Cavalieri, J.C. Comiso, C.L. Parkinson, and H.J. Zwally, *Arctic and Antarctic Sea Ice, 1978–1987: Satellite Passive-Microwave Observations and Analysis*, Nat. Aeronaut. and Space Admin., Washington, D. C., 1992.
- Goodwin, I.D., Firn core data from shallow drilling investigations in eastern Wilkes Land, East Antarctica, *Aust. Nat. Antarct. Res. Exped. Res. Notes* **65**, 74 pp., Aust. Antarct. Div., Kingston, Tasmania, Australia, 1988.
- Gow, A.J., Depth-time-temperature relationships of ice crystal growth in polar glaciers, *Res. Rep.* **300**, 19 pp., Cold Reg. Res. and Eng. Lab., Hanover, N. H., 1971.
- Gurvich, A.S., and T.G. Krasil'nikova, The polarization of the thermal radiation of permanent snow fields from measurements obtained from the 'Meteor' satellite, *Radio Eng. Electr. Phys.*, Engl. Transl., **22**, 88–94, 1977.
- Gurvich, A.S., V.I. Kalinin, and D.T. Matveyev, Influence of the internal structure of glaciers on their thermal radio emission, *Izv., Acad. Sci., USSR, Atmos. Oceanic Phys.*, Engl. Transl., **9**, 713–717, 1973.
- Joughin, I., M. Fahnestock, S. Ekhholm, and R. Kwok, Balance velocities of the Greenland ice sheet, *Geophys. Res. Lett.*, **24**, 3045–3048, 1997.
- Kieffer, H.H., H<sub>2</sub>O grain size and the amount of dust in Mars' residual north polar cap, *J. Geophys. Res.*, **95**, 1481–1493, 1990.
- Krinner, G., C. Genthon, Z.-X. Li, and P.L. Van, Studies of the Antarctic climate with a stretched-grid general circulation model, *J. Geophys. Res.*, **102**, 13,731–13,745, 1997.
- Mätzler, C., Applications of the interaction of microwave with natural snow cover, *Remote Sens. Rev.*, **2**, 259–387, 1987.
- Morse, D.L., E.D. Waddington, H.-P. Marshall, T.A. Neuman, E.J. Steig, J.E. Dibb, D.P. Winebrenner, and R.J. Arthern, Accumulation rate measurements at Taylor Dome, East Antarctica: Techniques and strategies for mass balance measurements in polar environments, *Geogr. Ann.*, **81A**, 683–694, 1999.
- Mote, T.L., and M.R. Anderson, Variations in snowpack melt on the Greenland ice sheet based on passive-microwave measurements, *J. Glaciol.*, **41**, 51–60, 1995.
- Oerlemans, J., and N.C. Hoogendoorn, Mass-balance gradients and climatic change, *J. Glaciol.*, **35**, 399–405, 1989.
- Ohmura, A., and N. Reeh, New precipitation and accumulation maps for Greenland, *J. Glaciol.*, **37**, 140–148, 1991.
- Paterson, W.S.B., *The Physics of Glaciers*, 3rd ed., 480 pp., Pergamon, New York, 1994.
- Percival, D.B., and A.T. Walden, *Wavelet Methods for Time Series Analysis*, 500 pp., Cambridge Univ. Press, New York, 2000.
- Rott, H., Multispectral microwave signatures of the Antarctic ice sheet, in *Microwave Radiometry Remote Sensing Applications*, edited by P. Pampaloni, pp. 89–101, VSP, Utrecht, the Netherlands, 1989.
- Rott, H., K. Sturm, and H. Miller, Active and passive microwave signatures of Antarctic firn by means of field measurements and satellite data, *Ann. Glaciol.*, **17**, 337–343, 1993.
- Shuman, C.A., and C.R. Stearns, Decadal length composite inland west Antarctic temperature records, *J. Clim.*, in press, 2001.
- Shuman, C.A., R.B. Alley, S. Anandakrishnan, J.W.C. White, P.M. Grootes, and C.R. Stearns, Temperature and accumulation at the Greenland Summit: Comparison of high-resolution isotope profiles and satellite passive microwave brightness temperature trends, *J. Geophys. Res.*, **100**, 9165–9177, 1995.
- Shuman, C.A., D.H. Bromwich, J. Kipfstuhl, and M. Schwager, Multiyear accumulation and temperature history near the NGRIP site, north central Greenland, *J. Geophys. Res.*, this issue.
- Shuman, C.A., R.B. Alley, M.A. Fahnestock, R.A. Bind-schadler, J.W.C. White, J. Winterie, and J.R. McConnell, Temperature history and accumulation timing for the snowpack at GISP2, central Greenland, *J. Glaciol.*, **44**, 21–30, 1998.
- Steffen, K., W. Abdalati, and I. Sherjal, Faceted crystal formation in the northeast Greenland low-accumulation region, *J. Glaciol.*, **45**, 63–68, 1999.
- Stephenson, P.J., Some aspects of shallow snow metamorphism at Southice, Antarctica, in *Proceedings of the International Symposium on Antarctic Glaciological Exploration (ISAGE)*, edited by A.J. Gow and others, International Association of Scientific Hydrology, Gentbrugge, Belgium, 1970.
- Surdyk, S., and M. Fily, Results of a stratified snow emissivity model based on the wave approach: Application to the Antarctic ice sheet, *J. Geophys. Res.*, **100**, 8837–8848, 1995.
- Thomas, R.H., T. Akins, B. Csatho, M. Fahnestock, P. Gogineni, C. Kim, and J. Sonntag, Mass balance of the Greenland ice sheet at high elevations, *Science*, **289**, 426–430, 2000.
- Tsang, L., J.A. Kong, and R.T. Shin, *Theory of Microwave Remote Sensing*, 613 pp., John Wiley, New York, 1985.
- Vaughan, D.G., J.L. Bamber, M. Giovinetto, J. Russell, and A.P.R. Cooper, Reassessment of the net surface mass balance in Antarctica, *J. of Clim.*, **12**, 993–946, 1999.
- Wahr, J., D. Wingham, and C. Bentley, A method of combined ICESAT and GRACE satellite data to constrain Antarctic mass balance, *J. Geophys. Res.*, **105**, 16,279–16,294, 2000.
- West, R.D., D.P. Winebrenner, L. Tsang, and H. Rott, Microwave emission from density-stratified Antarctic firn at 6 cm wavelength, *J. Glaciol.*, **42**, 63–76, 1996.
- Winebrenner, D.P., and R.J. Arthern, Satellite observation of Antarctic ice sheet accumulation rates and compari-

- son with regressions commonly used in ice-sheet modeling, 297–299 in *Proceedings of the ACSYS Conference on Polar Processes and Global Climate*, edited by K. Aagaard, Clim. Res. Program Doc. 106, WMO Tech. Doc. 908, World Meteorol. Org., Geneva, Switzerland, 1998.
- Zhang, H., L. Toudal Pederson, and P. Gudmandsen, Microwave brightness temperatures of the Greenland ice sheet, *Adv. Space. Res.*, 1, 227–287, 1989.
- Zwally, H.J., Microwave emissivity and accumulation rate of polar firn, *J. Glaciol.*, 18, 195–215, 1977.
- Zwally, H.J., and M.B. Giovinetto, Accumulation in Antarctica and Greenland derived from passive-microwave data: A comparison with contoured compilations, *Ann. Glaciol.*, 21, 123–130, 1995.
- 
- D.P. Winebrenner, Applied Physics Laboratory, Box 355640, University of Washington, Seattle, WA 98195, USA. (dpw@apl.washington.edu)
- R.J. Arthern, British Antarctic Survey, High Cross, Maddingley Rd., Cambridge CB3 0ET, United Kingdom. (rart@pcmail.nerc-bas.ac.uk)
- C.A. Shuman, Earth System Science Interdisciplinary Center, University of Maryland, College Park, MD 20742, USA (shuman@buggam.umd.edu)

(Received August 25, 2000; revised April 2, 2001; accepted April 5, 2001.)